Bol. Soc. Paran. Mat.
©SPM – E-ISSN-2175-1188
SPM: www.spm.uem.br/bspm

(3s.) **v. 2025 (43)** : 1–19.
ISSN-0037-8712
doi:10.5269/bspm.77845

Impact of Chemical Reaction on Three-Dimensional Casson Nanofluid Flow over a Rotating Surface with Prescribed Heat Flux, Viscous Dissipation, and Heat Source/Sink Effects

V. Meenakshi, S. Renuka, P. Sreehari, Santoshi Misra and G. Sreedhar Sarma*

ABSTRACT: This work explores the heat transfer behavior and three-dimensional flow of a Casson nanofluid over a continuously stretching flat surface within a rotating reference frame, accounting for the effects of chemical reaction and thermal source or sink. The analysis is based on the Buongiorno nanofluid model, incorporating viscous dissipation and a constant heat flux condition at the surface. To handle the complexity of the nonlinear partial differential equations, the study employs the non-Newtonian Casson fluid model alongside the boundary layer approximation. The governing equations are transformed into a dimensionless form and solved numerically using the shooting technique combined with the Adam's Moulton method, programmed in Fortran. A comprehensive parametric study is carried out to investigate the impacts of various dimensionless parameters on velocity profiles, temperature distribution, concentration fields, and engineering quantities such as the Nusselt number, skin friction, and Sherwood number. The results demonstrate strong agreement with previously published studies under specific limiting cases. The findings of this research have significant applications in various engineering and industrial fields. Specifically, they are crucial for designing advanced cooling systems for high-temperature rotating machinery, such as gas turbines and rotating heat exchangers used in aerospace and power generation industries. The inclusion of chemical reaction effects, heat source/sink mechanisms, and non-Newtonian fluid behavior makes this study relevant to enhanced cooling technologies for rotating electrical machines, nuclear reactors, and energy storage systems. Moreover, the results can be utilized in biomedical applications involving nanofluid transport in rotating systems, such as targeted drug delivery devices and blood flow modelling in rotating biological environments.

Key Words: Casson nanofluid, heat flux, chemical reaction, heat source or sink.

Contents

1. Introduction

The study of non-Newtonian fluids has gained significant attention in recent years due to their widespread applications in industries such as bioengineering, polymer processing, food production, and ink manufacturing. One of the most prominent non-Newtonian models is the Casson fluid, initially proposed by Casson [1] to describe the flow behavior of pigment-oil suspensions in printing inks. The Casson model accounts for yield stress behavior, making it highly suitable for complex fluids.

The concept of enhancing the thermal conductivity of base fluids by suspending nanoparticles was pioneered by Choi and Eastman [2], leading to the development of nanofluids, which show superior thermal properties compared to conventional fluids. This innovation has opened new avenues for improving heat transfer in various engineering systems.

Research on Casson fluids has expanded to include heat and mass transfer phenomena under diverse physical effects. Ramesh and Devakar [3] studied Casson fluid flow over an exponentially stretching surface considering viscous dissipation and Joule heating, revealing significant impacts on thermal profiles.

* Corresponding author.
2010 *Mathematics Subject Classification:* 76A05, 76U05, 76N20, 76W05, 80M25.
Submitted July 14, 2025. Published September 30, 2025

Furthermore, Khan and Pop [4] introduced boundary layer flow analysis of nanofluids over stretching sheets, underscoring the importance of nanoparticle dynamics in thermal systems. Studies like Makinde [5] and Das and Arifuzzaman [6] incorporated convective boundary conditions, chemical reactions, and non-linear thermal effects in Casson nanofluid models.

Heat transfer mechanisms in Casson fluid flows have been further investigated by Bhattacharyya [7], focusing on viscous dissipation and internal heat generation. More recent studies by Al-Kouz and Owhaib [8] and Saeed *et al.* [9] considered three-dimensional (3D) Casson nanofluid flows over rotating frames and inclined rotating disks, especially under the influence of heat generation/absorption and thermal radiation. These works emphasized the combined effect of rotation, nanoparticle suspension, and non-linear heat sources/sinks.

The analysis of Casson-Carreau hybrid models by Naga Santoshi *et al.* [10] and rotating nanofluid flows by Owhaib *et al.* [11] has further highlighted the influence of magnetic fields, radiation, and viscous heating. Ramzan *et al.* [12] explored dusty Casson nanofluid dynamics under variable heat sources/sinks, while Sreedhar Sarma *et al.* [13] and Ramanjana Koka *et al.* [14] studied the combined effects of magnetohydrodynamics (MHD) and radiation on chemically reactive nanofluid flows.

Moreover, Sharanayya and Biradar [15] and Reddy *et al.* [16] investigated chemical reactions and porous media effects, revealing intricate thermal and solutal interactions. Contributions by Sreedhar *et al.* [17] and Rasekh *et al.* [18] emphasized non-uniform heat sources and three-dimensional effects on Casson nanofluid flows. Raju *et al.* [19] and Prabhakar *et al.* [20] integrated second-order slip conditions and thermal slip to enhance modelling accuracy.

Recent studies like Sreedhar Sarma *et al.* [21], Ahmed *et al.* [22], and Manvi *et al.* [23] focused on unsteady three-dimensional Casson fluid dynamics with heat source/sink phenomena. Waheed *et al.* [24] presented unsteady MHD squeezing flow with thermal radiation and porous media effects, further broadening the understanding of complex Casson nanofluid behaviors.

Investigations by Reddy *et al.* [25], Sarma *et al.* [26], and Durgaprasad *et al.* [27] demonstrated that the interplay between thermal radiation, chemical reaction, porous media, and nanofluid properties significantly affects the momentum and thermal boundary layers. Additionally, Shehzad *et al.* [28] addressed three-dimensional MHD Casson fluid flows through porous media, revealing crucial insights into heat generation and nanoparticle behavior.

Motivated by these advancements, this study explores the three-dimensional Casson nanofluid flow over a rotating frame under prescribed heat flux, incorporating viscous heating, chemical reaction, and non-uniform heat source/sink effects. By employing a comprehensive mathematical model that captures the essential physical effects, this work aims to extend the understanding of Casson nanofluid flows in complex thermal environments, relevant to industrial processes involving rotating machinery, chemical reactors, and energy systems

2. Mathematical formulation

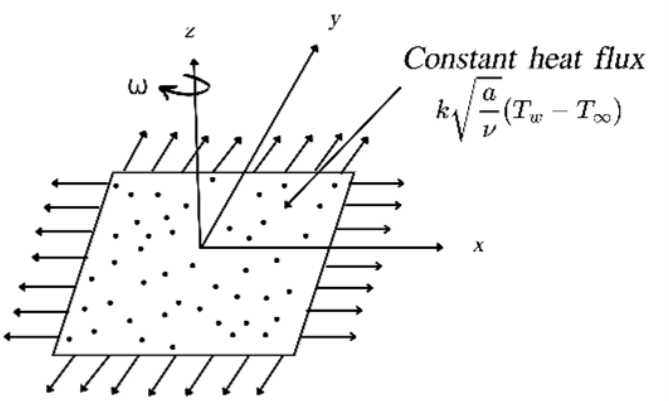

Figure 1: Flow diagram

This paper investigates the laminar, steady-state, three-directional flow of an extended non-Newtonian Casson nanofluid surface across a rotating frame. At the boundary, the nano liquid's surface is subjected to a constant surface heat flux. The Cartesian coordinate framework aligns with the xy-plane and considers the fluid region at $z \geq 0$. The incompressible Casson nano liquid spins uniformly at a rate ω about the z-axis. Figure 1 depicts a schematic depiction of the problem being investigated.

Using Prandtl's boundary layer technique, the current problem under consideration governing equations are defined as follows [8].

$$\frac{\partial u}{\partial x} + \frac{\partial v}{\partial y} + \frac{\partial w}{\partial z} = 0, \tag{2.1}$$

$$\rho\left(u\frac{\partial u}{\partial x} + v\frac{\partial u}{\partial y} + w\frac{\partial u}{\partial z} - 2\omega v\right) = \mu\left(1 + \frac{1}{\beta}\right)\frac{\partial^2 u}{\partial z^2}, \tag{2.2}$$

$$\rho\left(u\frac{\partial v}{\partial x} + v\frac{\partial v}{\partial y} + w\frac{\partial v}{\partial z} + 2\omega u\right) = \mu\left(1 + \frac{1}{\beta}\right)\frac{\partial^2 v}{\partial z^2}, \tag{2.3}$$

$$\rho C_p\left(u\frac{\partial T}{\partial x} + v\frac{\partial T}{\partial y} + w\frac{\partial T}{\partial z}\right) = k\frac{\partial^2 T}{\partial z^2} + (\rho C_p)_{np}\left\{D_B\frac{\partial T}{\partial z}\frac{\partial C}{\partial z} + \frac{D_T}{T_\infty}\left(\frac{\partial T}{\partial z}\right)^2\right\}$$
$$+\mu\left(1 + \frac{1}{\beta}\right)\left(\left(\frac{\partial u}{\partial z}\right)^2 + \left(\frac{\partial v}{\partial z}\right)^2\right) - Q_0(T - T_\infty) \tag{2.4}$$

$$u\frac{\partial C}{\partial x} + v\frac{\partial C}{\partial y} + w\frac{\partial C}{\partial z} = D_B\frac{\partial^2 C}{\partial z^2} + \frac{D_T}{T_\infty}\frac{\partial^2 T}{\partial z^2} - Kr(C - C_\infty) \tag{2.5}$$

where β-nondimensional Casson fluid parameter, u, v, and w are velocities along x, y and z- directions, $\nu = \frac{\mu}{\rho}$ is the kinematic viscosity, μ- dynamic viscosity, ρ- density, T- temperature, C- nanoparticle concentration, $\alpha = \frac{\kappa}{\rho C_p}$ is the thermal diffusivity, κ- thermal conductivity, ρC_p- specific heat of the Casson fluid, $(\rho C_p)_{np}$- specific heat of the nanoparticles, D_B- coefficient of Brownian diffusion, D_T- coefficient of thermos-migration diffusion and T_∞- ambient temperature.

The pertinent boundary conditions are

$$w = v = 0,\ u = U_w = ax,\ -k\left(\frac{\partial T}{\partial z}\right) = q_w,\ C = C_w \ \ at\ z = 0,$$

$$v = 0,\ u = 0,\ T = T_\infty,\ C = C_\infty \ \ as\ z \to \infty \tag{2.6}$$

Here a is stretching rate and $q_w = (T_w - T_\infty)\, k\sqrt{a/\nu}$ - constant heat flux.
By considering

$$\eta = z\sqrt{\frac{u_w}{x\nu}},\ u = axf'(\eta),\ v = axg(\eta),\ w = -\sqrt{\nu a}f(\eta),$$
$$T = (T_w - T_\infty)\,\theta(\eta) + T_\infty,\quad C = (C_w - C_\infty)\,\phi(\eta) + C_\infty \tag{2.7}$$

Equation (2.1) is fulfilled and the remaining Equations (2.2) - (2.6) produce

$$\left(1+\frac{1}{\beta}\right)f''' + ff'' - (f')^2 + 2R_0 g = 0 \tag{2.8}$$
$$\left(1+\frac{1}{\beta}\right)g'' + fg' - gf' - 2R_0 f' = 0 \tag{2.9}$$
$$\frac{1}{Pr}\theta'' + f\theta' + Nb\theta'\phi' + Nt\ \phi'^2 + Ec\left(1+\frac{1}{\beta}\right)\left((f'')^2 + (g')^2\right) + Q\theta = 0 \tag{2.10}$$
$$\phi'' + \frac{Nt}{Nb}\theta'' + Lef\phi' - KrLe\phi = 0 \tag{2.11}$$

Corresponding boundary conditions are

$$f = 0,\ g = 0,\ f' = 1,\ \theta' = -1,\ \phi = 1\ at\ \eta = 0$$
$$f' = 0,\ f = 0,\ \theta = 0,\ \phi = 0\ as\ \eta \to \infty \tag{2.12}$$

where η -similarity variable, f, g, θ and ϕ are dimensionless primary velocity, transverse velocity, temperature, and nanoparticle concentration respectively, $Pr = \frac{C_p\mu}{\kappa}$ the Prandtl number, $R_0 = \frac{\omega}{a}$ the Rotation parameter, $Le = \frac{\nu}{D_B}$ the Lewis number, $Nt = \frac{(\rho C_p)_{np} D_{T(T_w - T_\infty)}}{\rho C_p\ T_\infty \nu}$ the Thermophoresis parameter, $Nb = \frac{(\rho C_p)_{np} D_{B(C_w - C_\infty)}}{\rho C_p\ \nu}$ the Brownian motion parameter,

$Ec = \frac{u_w}{C_{Pl}(T_w - T_\infty)}$ the Eckert number, $Kr = \frac{Kr}{a}$ the Chemical reaction parameter and $Q = \frac{Q_0}{\rho C_p}$ the Heat souce/sink parameter.

The following are the dimensionless expressions for Skin friction, Nusselt number, and Sherwood number.

$$Re_x{}^{1/2} Sf_x = \left(1+\frac{1}{\beta}\right)f''(0),\quad Re_y{}^{1/2} Sf_y = \left(1+\frac{1}{\beta}\right)g''(0),$$
$$Re_x{}^{-1/2} Nu_x = -\theta'(0),\quad Re_x{}^{-1/2} Sh_x = -\phi'(0) \tag{2.13}$$

where $Re_x = \frac{u_w(x)x}{\nu_l}$ is Reynolds number.

3. Methodology of Solution

Due to their coupled and nonlinear nature, the system of equations (2.8) - (2.11) and their boundary conditions (2.12) cannot be solved analytically. Using the Adams-Bashforth Moulton method and the Shooting approach, these nonlinear coupled ordinary differential equations are numerically solved. In order to use this strategy, we first transform the higher-order ODE system into a first-order ODE system. The following is a rewrite of equations (2.8) - (2.11):

$$f''' = \left(\frac{\beta}{1+\beta}\right)\left[-ff'' + (f')^2 - 2R_0 g\right] \tag{3.1}$$
$$g'' = \left(\frac{\beta}{1+\beta}\right)\left[-fg' + gf' + 2R_0 f'\right] \tag{3.2}$$
$$\theta'' = Pr\left[-f\theta' - Nb\theta'\phi' - Nt\ \phi'^2 - Ec\left(1+\frac{1}{\beta}\right)\left((f'')^2 + (g')^2\right) - Q\theta\right] \tag{3.3}$$
$$\phi'' = -\frac{Nt}{Nb}\theta'' - Lef\phi' + KrLe\phi \tag{3.4}$$

By using the following notations,
Let $f = h_1,\ f' = h_2,\ f'' = h_3,\ g = h_4,\ g' = h_5,\ \theta = h_6,\ \theta' = h_7,\ \phi = h_8, \phi' = h_9$

$$h_1' = h_2, \quad h_1(0) = 0 \tag{3.5}$$
$$h_2' = h_3, \quad h_2(0) = 1 \tag{3.6}$$
$$h_3' = \left(\frac{\beta}{1+\beta}\right)\left[-h_1 h_3 + (h_2)^2 - 2R_0 h_4\right], \quad h_3(0) = H_3 \tag{3.7}$$
$$h_4' = h_5, h_4(0) = 0 \tag{3.8}$$
$$h_5' = \left(\frac{\beta}{1+\beta}\right)\left[-h_1 h_5 + h_4 h_2 + 2R_0 h_2\right], \quad h_5(0) = H_5 \tag{3.9}$$
$$h_6' = h_7, \quad h_6(0) = H_6 \tag{3.10}$$
$$h_7' = Pr\left[-h_1 h_7 - Nb h_7 h_8 - Nt\ {h_8}^2 - Ec\left(1 + \frac{1}{\beta}\right)\left((h_3)^2 + (h_5)^2\right) - Q h_6\right], \ h_7(0) = -1 \tag{3.11}$$
$$h_8' = h_9, \quad h_8(0) = 1 \tag{3.12}$$
$$h_9' = -\frac{Nt}{Nb} h_7' - Lef h_9 + KrLe h_8, \quad h_9(0) = H_9 \tag{3.13}$$

Where H_3, H_5, H_6, H_9 are the initial guesses. To solve the system of above first order ordinary differential equations, the unbounded domain $[0, \infty]$ is restricted to a bounded domain $[0, \eta]$ for some suitable choice of η. In the modelled problem, H_3, H_5, H_6, H_9 are initial guesses which are required to solve the above first order system of ODEs with the Adams-Bashforth Moulton method. The shooting method requires some initial guesses for H_3, H_5, H_6, H_9. The initial guesses are updated by the Newton's method until a solution of the problem which approximately meets the given boundary conditions at the right end of the domain.

The missing initial conditions H_3, H_5, H_6, H_9 are to be chosen such that

$$h_3(\eta, H_3, H_5, H_6, H_9) = 0$$
$$h_5(\eta, H_3, H_5, H_6, H_9) = 0$$
$$h_6(\eta, H_3, H_5, H_6, H_9) = 0$$
$$h_9(\eta, H_3, H_5, H_6, H_9) = 0$$

To start the iterative process, choose $H_3 = H_{3_0}, H_5 = H_{5_0}, H_6 = H_{6_0}, H_9 = H_{9_0}$. To the values of H_3, H_5, H_6, H_9 Newton's iterative scheme has been applied.

$d^* = e^* - J^{-1} g$, where

$$d^* = \begin{bmatrix} {H_3}^{(n+1)} \\ {H_5}^{(n+1)} \\ {H_6}^{(n+1)} \\ {H_9}^{(n+1)} \end{bmatrix}, e^* = \begin{bmatrix} {H_3}^{(n)} \\ {H_5}^{(n)} \\ {H_6}^{(n)} \\ {H_9}^{(n)} \end{bmatrix}, J = \begin{bmatrix} \frac{\partial h_3}{\partial H_3} & \frac{\partial h_3}{\partial H_5} & \frac{\partial h_3}{\partial H_6} & \frac{\partial h_3}{\partial H_9} \\ \frac{\partial h_5}{\partial H_3} & \frac{\partial h_5}{\partial H_5} & \frac{\partial h_5}{\partial H_6} & \frac{\partial h_5}{\partial H_9} \\ \frac{\partial h_6}{\partial H_3} & \frac{\partial h_6}{\partial H_5} & \frac{\partial h_6}{\partial H_6} & \frac{\partial h_6}{\partial H_9} \\ \frac{\partial h_9}{\partial H_3} & \frac{\partial h_9}{\partial H_5} & \frac{\partial h_9}{\partial H_6} & \frac{\partial h_9}{\partial H_9} \end{bmatrix}, g = \begin{bmatrix} {h_3}^{(n+1)} \\ {h_5}^{(n+1)} \\ {h_6}^{(n+1)} \\ {h_9}^{(n+1)} \end{bmatrix}$$

The convergence conditions are set so that subsequent values agree up to three significant digits. The decision of $\eta = 10$ was sufficient for the final conditions.

4. Interpretations of Results

The system of nonlinear differential equations (2.8)-(2.11) with boundary conditions (2.12) was solved numerically by combining the shooting approach with Adam's Moulton method. The Fortran language was used to perform the calculations. Various physical parameters are calculated numerically for a range of values, including the following: the rotation parameter, the Brownian motion parameter, the Lewis number, the Casson parameter, the chemical reaction parameter, the heat source or sink parameter, the thermophoresis parameter, the Eckert number, the Prandtl number, the Skin friction coefficients at the plate, the Sherwood number, and the Nusselt number.

Code Validation:

To ensure the accuracy of the numerical scheme employed, the computed values of $-\theta'(0)$ were compared with those reported in Khan and Pop [4] and Wael Al-Kouz and Wahib Owhaib [8] as shown in Table 1, demonstrating very good agreement.

Table 1: Comparison of $-\theta'(0)$ for $Nb = Nt = Q = Kr = \phi = 0$

P_{rl}	Khan and Pop [4]	Wael Al-Kouz and Wahib Owhaib [8]	Present Result
0.07	0.0663	0.06562	0.064998521
0.2	0.1691	0.16909	0.168598124
0.7	0.4539	0.45392	0.449844132
2	0.9113	0.91136	0.911266321
7	1.8954	1.89542	1.895434387

Table 2 displays the values of skin friction along x, y directions and Sherwood number for various non-dimensional parameters. It is observed that an increase in the Rotation parameter R_0 results in reduced axial skin friction and increased transverse skin friction due to Coriolis effects. The Sherwood number increases significantly with increasing Kr, indicating more efficient mass transfer. The Sherwood number ${Re_x}^{-\frac{1}{2}} Sh_x$ increases with increase of Ec, Q, Nt, Nb and decreases with the increase of Prandtl number, Casson parameter and Rotation parameter.

Table 2: Results of the ${Re_x}^{\frac{1}{2}} S_{f,x}$, ${Re_x}^{\frac{1}{2}} S_{f,y}$ and ${Re_x}^{-\frac{1}{2}} Sh_x$for various parameters

Pr	Ec	β	Q	R_0	Le	Nt	Nb	Kr	${Re_x}^{\frac{1}{2}} S_{f\,x}$	${Re_x}^{\frac{1}{2}} S_{f\,y}$	${Re_x}^{-\frac{1}{2}} Sh_x$
0.5	0.2	0.2	0.1	0.5	1	0.5	0.5	0.5	-3.02688	1	0.941704
0.6									-3.02688	1	0.922552
0.7									-3.02688	1	0.909939
1	0.0	0.2	0.1	0.5	1	0.5	0.5	0.5	-3.30792	1	0.741355
	0.1								-3.30792	1	0.846384
	0.2								-3.30792	1	0.951874
1	0.2	0.1	0.1	0.5	1	0.5	0.5	0.5	-4.28822	1	0.953252
		0.2							-2.85946	1	0.891877
		0.3							-2.3391	1	0.871528
1	0.2	0.2	-0.1	0.5	1	0.5	0.5	0.5	-5.08797	1	1.93874
			0.0						-5.08797	1	2.65612
			0.1						-5.08797	1	4.39941
1	0.2	0.2	0.1	0.1	1	0.5	0.5	0.5	-3.82328	0.2	4.75245
				0.2					-3.82585	0.4	1.97775
				0.3					-3.83015	0.60	1.49712
1	0.2	0.2	0.1	0.5	0.1	0.5	0.5	0.5	-3.02688	1	-0.267021
					0.2				-3.02688	1	-0.0684199
					0.3				-3.02688	1	0.102875
1	0.2	0.2	0.1	0.5	1	0.1	0.5	0.5	-3.30792	1	0.970053
						0.2			-3.30792	1	0.971548
						0.3			-3.30792	1	0.969558
1	0.2	0.2	0.1	0.5	1	0.5	0.5	0.5	-3.30792	1	0.951874
							0.7		-3.30792	1	1.029
							0.9		-3.30792	1	1.07726
1	0.2	0.2	0.1	0.5	1	0.5	0.5	0.5	-3.02688	1	0.89721
								0.7	-3.02688	1	1.0937
								0.9	-3.02688	1	1.26756

The impact of several non-dimensional parameters on temperature, concentration, and velocity profiles is shown in the following graphs.

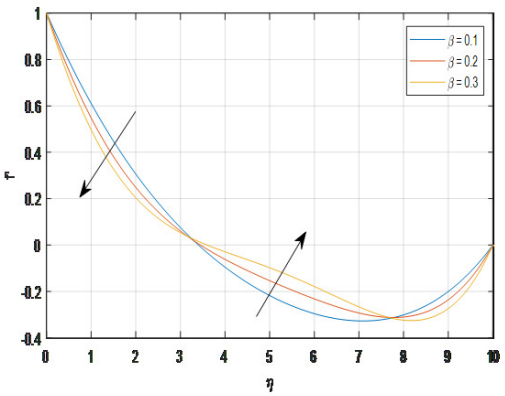

Figure 2: Change in f' with varying β

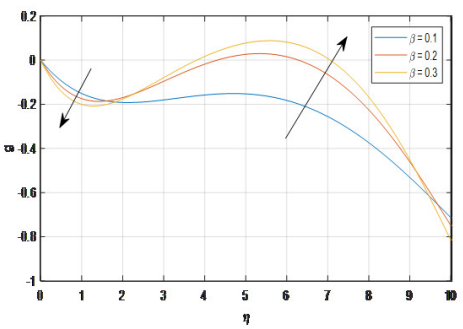

Figure 3: Change in g with varying β

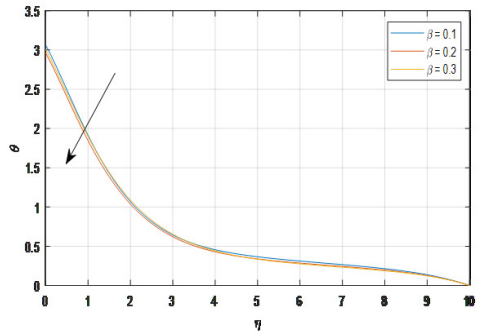

Figure 4: Change in θ with varying β

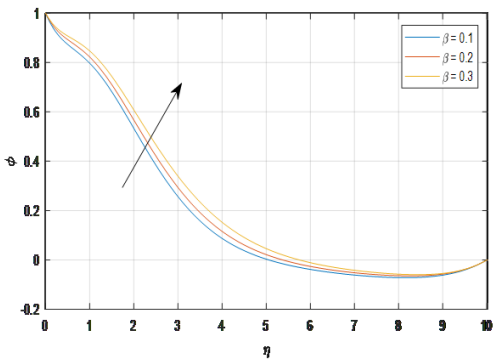

Figure 5: Change in ϕ with varying β

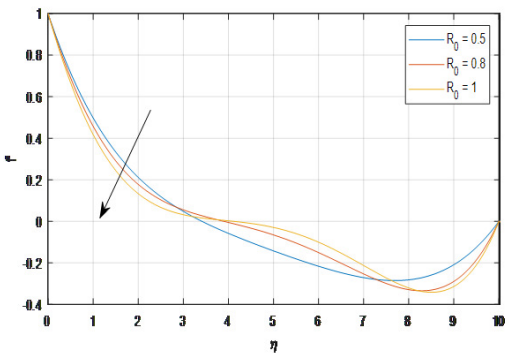

Figure 6: Change in f' with varying R_0

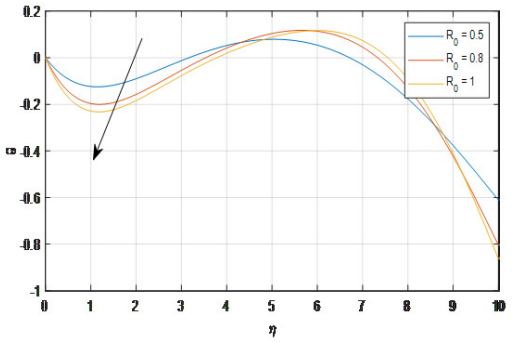

Figure 7: Change in g with varying R_0

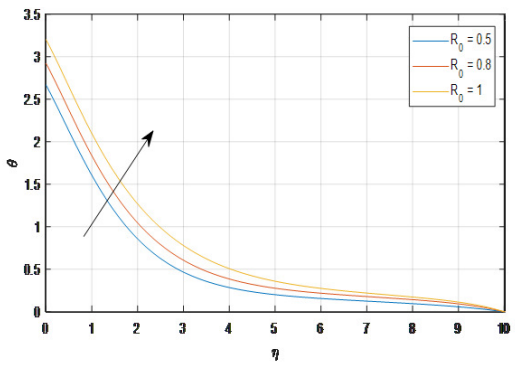

Figure 8: Change in θ with varying R_0

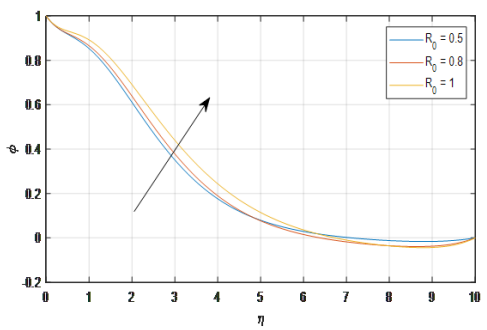

Figure 9: Change in ϕ with varying R_0

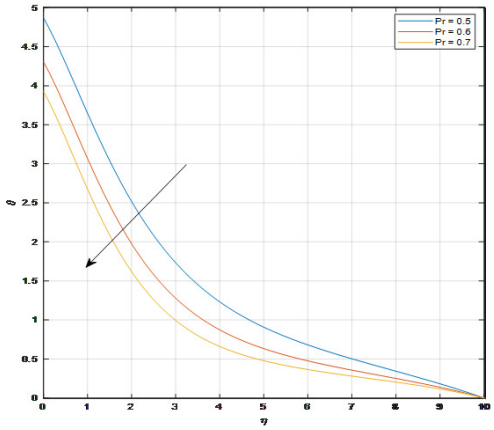

Figure 10: Change in θ with varying Pr

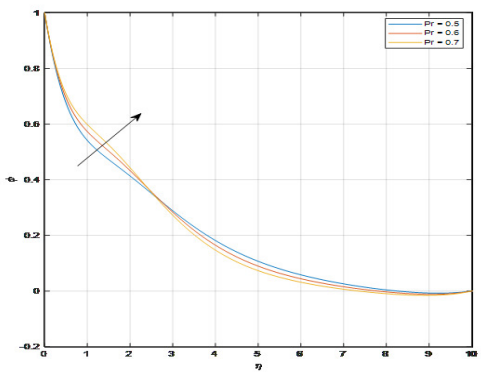

Figure 11: Change in ϕ with varying Pr

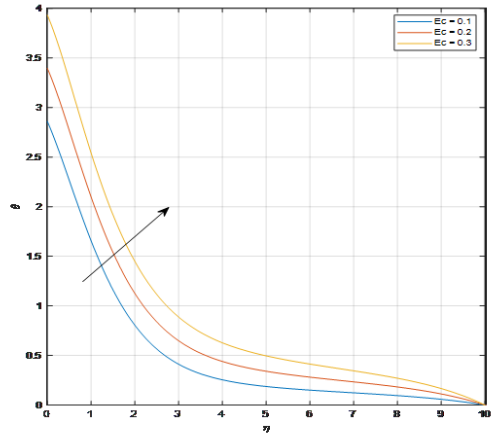

Figure 12: Change in θ with varying Ec

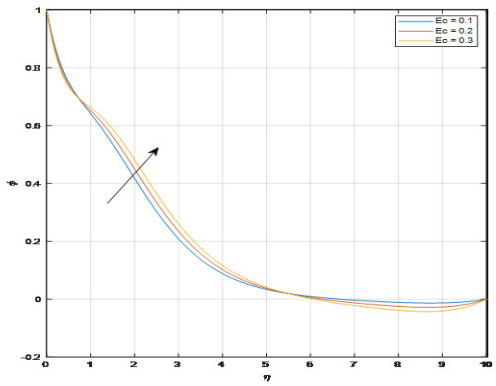

Figure 13: Change in ϕ with varying Ec

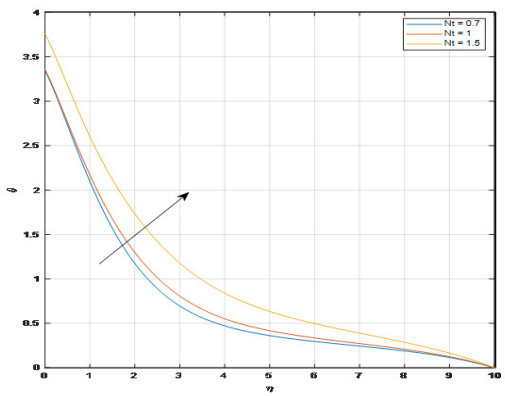

Figure 14: Change in θ with varying Nt

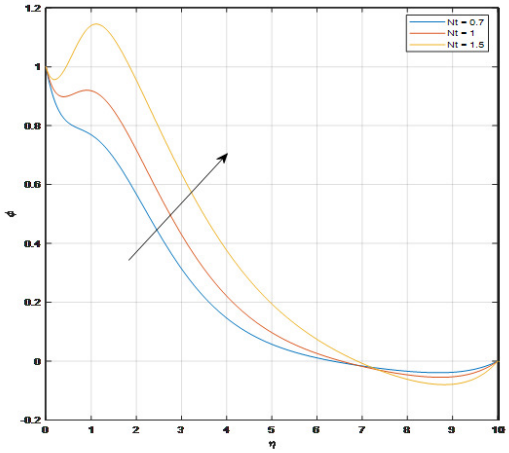

Figure 15: Change in $\phi$with varying Nt

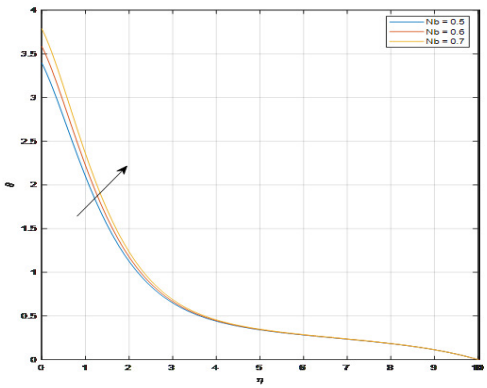

Figure 16: Change in θ with varying Nb

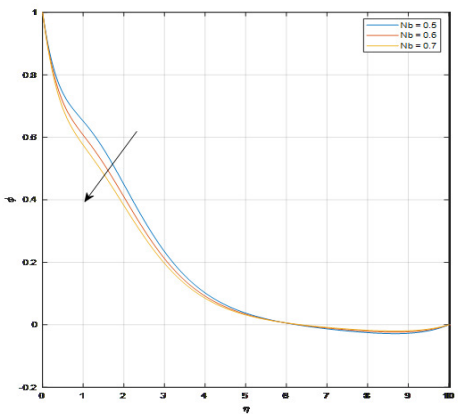

Figure 17: Change in ϕ with varying Nb

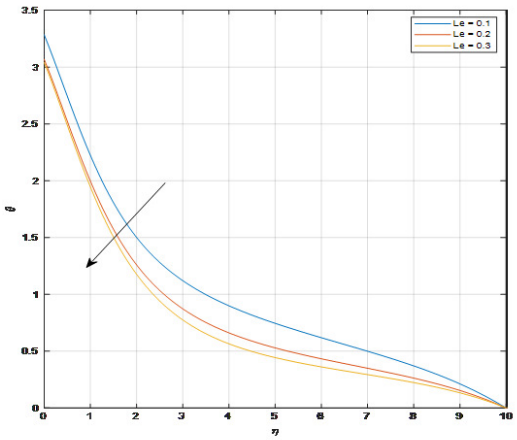

Figure 18: Change in θ with varying Le

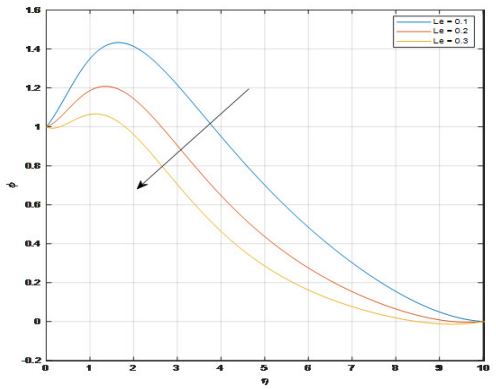

Figure 19: Change in ϕ with varying Le

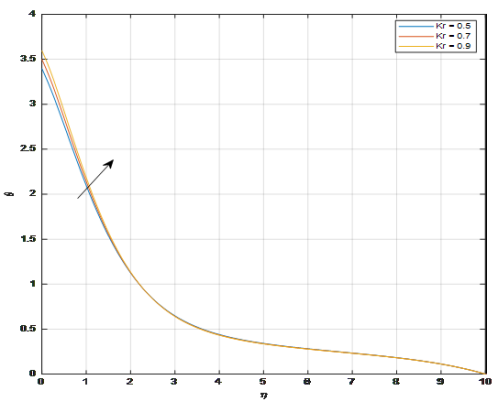

Figure 20: Change in θ with varying Kr

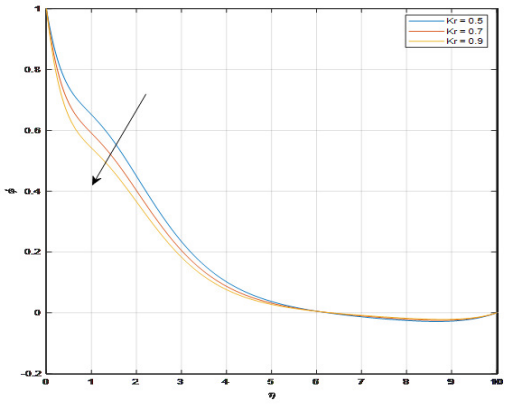

Figure 21: Change in ϕ with varying Kr

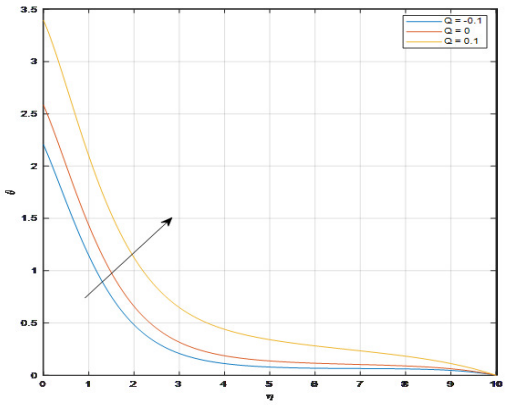

Figure 22: Change in θ with varying Q

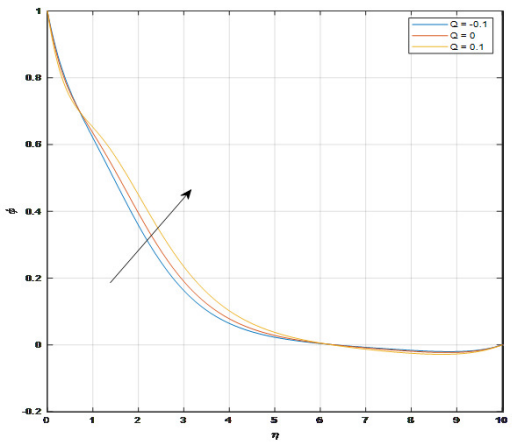

Figure 23: Change in ϕ with varying Q

Casson Parameter:

The axial velocity profile f' in Figure 2 exhibits a decreasing tendency when β is low and gradually increases when β increases since the fluid transitions towards Newtonian behaviour, reducing resistance to flow and increasing the primary velocity in the x-direction. When β is lower, the transverse velocity decreases and increasing behaviour is observed for larger β in Figure 3 since it reduces the yield stress influence, promoting stronger transverse flow induced by the rotating surface. As shown in Figures 4 and 5, the thickness of the thermal boundary layer is diminished as β becomes greater and reverse trend is observed in nanoparticle concentration.

Rotation Parameter:

Figures 6, 7, 8 and 9 demonstrate the effects of Rotation parameter R_0 on dimensionless velocities f', g, temperature θ and nanoparticle concentration ϕ. The ratio of the angular velocity rate to the elongating velocity rate is known as a rotation parameter. As it is noticed in Figures 6 and 7, higher values of the Rotation parameter correspond to a smaller elongating velocity rate, that is, the Coriolis forces become stronger, creating a rotational effect that reduces the velocity component. Consequently, the magnitude of velocities is decreased by rising values of R_0. Figures 8 and 9 show that the temperature and nanoparticle concentration increase with the increase of Rotation parameter. Rotational motion raises viscous dissipation, thereby increasing fluid temperature and thickening the thermal boundary layer and it also suppress convective mass transport by thickening the concentration boundary layer.

Prandtl number:

The effect of Prandtl number is illustrated in Figures 10 and 11. Higher Pr implies lower thermal diffusivity, causing a steeper temperature gradient and thinner thermal boundary layer. Thus, $\theta(\eta)$ decreases with increasing Pr. As Pr grows from Figure 11, the nano particle concentration $\phi(\eta)$ rises close to the plate and falls distant from it due to less thermophoretic motion of nanoparticles.

Eckert number:

Ec represents viscous dissipation. As Ec increases, more thermal energy is generated within the fluid, raising the fluid temperature. The thermal boundary layer thickens in Figure 12. It is observed from Figure 13 that, thermophoretic forces becomes stronger, hence nanoparticles move more vigorously away from the hot surface. This increases the concentration in the fluid region.

Thermophoresis parameter:

The impact of Nt is illustrated in Figures 14 and 15. Higher Nt increases thermal transport from the wall region, thickening the thermal boundary layer and raising $\theta(\eta)$. When thermophoresis parameter rises, it increases nanoparticle migration from hot to cold regions, generally increasing in concentration is observed. This phenomenon is widely used in particle separation, semiconductor processing, and environmental control.

Brownian motion parameter:

Larger Nb enhances nanoparticle motion and energy transfer, increasing the temperature is shown in Figure 16. From Figure 17, it is observed that, increased Nb elevates mass diffusion of nanoparticles, decreasing the concentration profile due to more rapid dispersion. Brownian motion plays a critical role in diffusion-based processes, affecting nanoparticle transport and stability such as pharmaceutical drug delivery and biomedicine, air filtration and aerosol transport.

Lewis number:

The influence of Le is depicted in Figures 18 and 19. Increasing the Lewis number suppresses the mass diffusion of nanoparticles, reducing the thermophoretic and Brownian heating effects. Consequently, the fluid temperature profile decreases, and the thermal boundary layer becomes thinner at higher Le values. The concentration profiles are also diminished due to slower mass diffusion relative to thermal diffusion.

Chemical reaction Parameter:

Figures 20 and 21 show the effect of the chemical reaction parameter Kr. Larger Kr enhances species consumption due to chemical reaction, reducing concentration and thinning the solutal boundary layer from Figure 21. The enhanced temperature profiles are noticed in Figure 20 as the chemical reaction parameter grows.

Heat Source/ Sink Parameter:

The impact of the heat source or sink parameter is drawn in Figures 22 to 23. It is observed from Figure 22 that, a positive Q(source) increases the internal heating, elevating the temperature, while a

negative Q(sink) reduces it. A rise in concentration profiles is seen in Figure 23 as the heat source or sink parameter increases.

5. Conclusions

A comprehensive analysis has been carried out to investigate the influence of various physical parameters on the three-dimensional Casson nanofluid flow over a rotating surface, considering prescribed heat flux, viscous dissipation, chemical reaction, and heat source/sink effects. The governing nonlinear differential equations were solved numerically, and the results were interpreted through variations in velocity, temperature, and concentration distributions. The key findings are summarized as follows:

1. An increase in R_0 enhances Coriolis effects, reducing both velocity components. However, it raises both temperature and concentration profiles by strengthening viscous dissipation and suppressing convective mass transport, resulting in thicker thermal and concentration boundary layers.

2. A decrease in β intensifies the non-Newtonian effects, reducing both axial and transverse velocities. Higher β (weaker Casson effect) promotes flow and reduces viscous resistance. The thermal boundary layer thickness decreases with β, while the nanoparticle concentration increases due to weakened internal shear and temperature gradients.

3. Viscous dissipation effects increase with higher Ec , causing a rise in fluid temperature and thickening the thermal boundary layer. The resulting stronger thermophoretic forces also increase nanoparticle concentration in the bulk fluid.

4. Stronger chemical reactions (higher Kr) intensify species depletion, decreasing the concentration and thinning the solutal boundary layer. Temperature profiles show an increasing trend with Kr due to enhanced reaction-induced thermal effects.

5. Temperature and concentration profiles climb when the Heat source or sink parameter rises.

6. As the thermophoresis parameter increased, the temperature and concentration profiles improved.

7. The Sherwood number increases significantly with increasing Kr, indicating more efficient mass transfer.

These insights are valuable for optimizing heat and mass transfer in rotating systems, nanofluid-based technologies, and industrial applications such as cooling systems, polymer processing, and chemical reactors. Future extensions of this work with other geometry and physical conditions are possible. This study may be extended to multi-phase flows, where the interaction between different phases can significantly affect the heat and mass transfer characteristics.

Acknowledgement

We appreciate the reviewer's important time in reading and commenting on this article. We really appreciate your thoughtful feedback and recommendations that might improve the article's quality. There is no grant funding for this work.

Nomenclature

u, v, w - Velocity components in $x,\ y\ and\ z$ directions	k -Thermal conductivity
T - Temperature of the fluid	σ^* - Stephen Boltzmann coefficient
α - Thermal diffusivity	k^* - Mean absorption constant
η - dimensionless similarity variable	α^* - Rosseland mean absorption coefficient
T_w - Fluid temperature at the surface	ω - Rotational velocity
a - Stretching rate	Ec Eckert number
T_∞ - Fluid temperature at infinity	Q - Heat source or sink parameter
f - Dimensionless axial velocity	Nu - Nusselt number
g - Dimensionless transverse velocity	Sh - Sherwood number
θ - dimensionless fluid temperature	Pr - Prandtl number
ϕ - Dimensionless nanoparticle concentration	Le - Lewis number
μ - Dynamic viscosity of the fluid	Kr - Chemical reaction parameter
ρ - Density of the fluid	D_B - Brownian diffusion coefficient
q_w - Constant heat flux	C_p - Specific heat
β - Casson fluid parameter	ρC_p - Casson fluid heat capacity
Re - Reynolds number	$(\rho C_p)_{np}$ - Nanoparticles heat capacity
C - Nano particle concentration	C_w - Plate nanoparticles concentration
ν - Kinematic viscosity	Nt - Thermophoresis parameter
R_0 - Rotation parameter	Nb - Brownian motion parameter
D_T - Thermo-migration diffusion coefficient	

References

1. Casson, N., *A flow equation for pigment-oil suspensions of the printing ink type*, Rheology of Disperse Systems, Pergamon Press, 84–104, (1959).
2. Choi, S. U. S., and Eastman, J. A., *Enhancing thermal conductivity of fluids with nanoparticles*, Proc. ASME Int. Mech. Eng. Congress and Exposition, 231, 99–105, (1995).
3. Ramesh, K., and Devakar, M., *Effects of viscous dissipation and Joule heating on Casson fluid flow past an exponentially stretching surface in the presence of thermal radiation*, Appl. Math. Comput. 271, 753–767, (2015).
4. Khan, W. A., and Pop, I., *Boundary-layer flow of a nanofluid past a stretching sheet*, Int. J. Heat Mass Transfer 53(11–12), 2477–2483, (2010).
5. Makinde, O. D., *Similarity solution of hydromagnetic heat and mass transfer over a vertical plate with a convective surface boundary condition*, Int. J. Phys. Sci. 6(6), 1508–1516, (2011).
6. Das, K., and Arifuzzaman, M., *Heat and mass transfer effects on Casson nanofluid flow over a stretching sheet with chemical reaction*, Alexandria Eng. J. 54(2), 251–261, (2015).
7. Bhattacharyya, K., *Heat transfer analysis in Casson fluid flow over a stretching surface with viscous dissipation and heat generation/absorption*, J. Mech. Eng. Sci. 225(11), 2587–2593, (2011).
8. Al-Kouz, W., and Owhaib, W., *Numerical analysis of Casson nanofluid three-dimensional flow over a rotating frame exposed to a prescribed heat flux with viscous heating*, Sci. Rep. 12, 4256, (2022). doi:10.1038/s41598-022-08211-2
9. Saeed, A., Shah, Z., Islam, S., Jawad, M., Ullah, A., Gul, T., and Kumam, P., *Three-dimensional Casson nanofluid thin film flow over an inclined rotating disk with the impact of heat generation/consumption and thermal radiation*, Coatings 9(4), 248, (2019).
10. Naga Santoshi, P., Ramana Reddy, G. V., and Padma, P., *Numerical scrutinization of three dimensional Casson-Carreau nanofluid flow*, J. Appl. Comput. Mech. 6(3), 531–542, (2020).
11. Owhaib, W., Basavarajappa, M., and Al-Kouz, W., *Radiation effects on 3D rotating flow of Cu-water nano liquid with viscous heating and prescribed heat flux using modified Buongiorno model*, Sci. Rep. 11, 20669, (2021).
12. Ramzan, M., Shaheen, N., Chung, J. D., et al., *Impact of Newtonian heating and Fourier and Fick's laws on a magnetohydrodynamic dusty Casson nanofluid flow with variable heat source/sink over a stretching cylinder*, Sci. Rep. 11, 2357, (2021). doi:10.1038/s41598-021-81747-x
13. Sreedhar Sarma, G., Narender, G., and Govardhan, K., *Radiation effect on the flow of Magneto Hydrodynamic nanofluids over a stretching surface with Chemical reaction*, J. Comput. Appl. Mech. 53(4), 494–509, (2022). doi:10.22059/jcamech.2022.348047.749
14. Ramanjana Koka, and Aruna Ganjikunta, *Investigating the Impact of Magnetohydrodynamic (MHD) and Radiation on the Casson-Based Nanofluid Flow over a Linear Stretching Sheet in a Porous Medium with Heat Source or Sink*, J. Adv. Res. Fluid Mech. Therm. Sci. 111(2), 170–194, (2023). doi:10.37934/arfmts.111.2.170194

15. Sharanayya, and Biradar, S., *Magnetized Dissipative Casson Nanofluid Flow over a Stretching Sheet with Heat Source/Sink and Soret Effect Under Porous Medium*, BioNanoScience, 1–19, (2023). doi:10.1007/s12668-023-01184-0

16. Reddy, J. V. R., Sugunamma, V., Sandeep, N., and Chakravarthula, S. K., *Chemically reacting MHD dusty nanofluid flow over a vertical cone with non-uniform heat source/sink*, Walailak J. Sci. Technol. (WJST) 14(2), 141–156, (2017).

17. Sreedhar Sarma, G., Narender, G., Dontula, S., Vishwaroju, R., and Reddy, M. G., *Analysis of Magneto Hydrodynamic Casson Nanofluid on an Inclined Porous Stretching Surface with Heat Source/Sink and Viscous Dissipation Effects: A Buongiorno Fluid Model Approach*, J. Adv. Res. Fluid Mech. Therm. Sci. 109(2), 151–167, (2023).

18. Rasekh, A., Ganji, D., and Tavakoli, S., *Numerical solutions for a nanofluid past over a stretching circular cylinder with non-uniform heat source*, Front. Heat Mass Transf. (FHMT) 3(4), (2013).

19. Raju, C. S., Sandeep, N., Ali, M. E., and Nuhait, A. O., *Heat and mass transfer in 3-D MHD Williamson–Casson fluids flow over a stretching surface with non-uniform heat source/sink*, Therm. Sci. 23(1), 281–293, (2019).

20. Prabhakar, B., Bandari, S., and Kumar, C. K., *Effects of inclined magnetic field and chemical reaction on flow of a Casson nanofluid with second order velocity slip and thermal slip over an exponentially stretching sheet*, Int. J. Appl. Comput. Math. 3(4), 2967–2985, (2017).

21. Gobburu, S. S., Subbaiah, G. V., Narender, G., Reddy, D. S., Shankaraiah, D., and Umakanth, M., *Exploring Unsteady Three-Dimensional Casson Fluid Flow through a Stretching Surface with Heat Source Sink: A Numerical Investigation*, J. Adv. Res. Fluid Mech. Therm. Sci. 118(1), 116–131, (2024). doi:10.37934/arfmts.118.1.116131

22. Ahmed, M., Yousaf, R. M., Hassan, A., et al., *Casson Nanofluid Flow with Cattaneo-Christov Heat Flux and Chemical Reaction Past a Stretching Sheet in the Presence of Porous Medium*, Front. Heat Mass Transf. 22(4), 1261–1276, (2024). doi:10.32604/fhmt.2024.048091

23. Manvi, B. K., Kerur, S. B., Tawade, J. V., Nieto, J. J., Sankeshwari, S. N., Ahmad, H., et al., *MHD Casson nanofluid boundary layer flow in presence of radiation and non-uniform heat source/sink*, Math. Model. Control 3, 152–167, (2023).

24. Waheed, S. E., Moatimid, G. M., and Elfeshawey, A. S., *Unsteady magnetohydrodynamic squeezing darcy-forchheimer flow of Fe_3O_4 Casson nanofluid: impact of heat source/sink and thermal radiation*, Partial Differ. Equ. Appl. Math. 10, 100666, (2024). doi:10.1016/j.padiff.2024.100666

25. Reddy, N. N., Rao, V. S., and Reddy, B. R., *Impact of thermal radiation and chemical reaction on MHD heat and mass transfer Casson nanofluid flow past a stretching sheet in presence of heat source/sink*, ARPN J. Eng. Appl. Sci. 16, 1165–1171, (2006).

26. Sarma, G. S., Narender, G., and Govardhan, K., *Comprehensive study of Buongiorno nanofluid model for MHD Casson flow on an inclined porous stretching surface with heat source/sink and viscous dissipation*, Z. Angew. Math. Mech. 104, (2024). doi:10.1002/zamm.202300362

27. Durgaprasad, P., Saleem, S., Varma, S. V. K., and Raju, C. S. K., *Three-dimensional slip flow of a chemically reacting Casson fluid flowing over a porous slender sheet with a non-uniform heat source or sink*, J. Korean Phys. Soc. 74(9), 855–864, (2019). doi:10.3938/jkps.74.855

28. Shehzad, S., Hayat, T., and Alsaedi, A., *Three-dimensional MHD flow of Casson fluid in porous medium with heat generation*, J. Appl. Fluid Mech. 9(1), 215–223, (2016). doi:10.18869/acadpub.jafm.68.224.24042

V. Meenakshi,
Department of technical education,
J N Government Polytechnic,
Hyderabad, Telangana, India.
E-mail address: adegajender1979@gmail.com

and

S. Renuka,
Department of Mathematics,
Nizam College, Osmania University,
Hyderabad, Telangana, India.
E-mail address: renuka.avr@gmail.com

and

P. Sreehari,
Department of Mathematics,

Osmania University,
Hyderabad, Telangana, India.
E-mail address: pagidipallysrihari@gmail.com

and

Santoshi Misra,
Department of Mathematics,
St Ann's College for Women,
Hyderabad, Telangana, India.
E-mail address: drsantoshishukla@gmail.com

and

G. Sreedhar Sarma,
Department of H&S(Mathematics),
CVR College of Engineering,
Hyderabad, Telangana, India.
E-mail address: sarma.sreedhar@gmail.com